
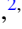









## Inelastic neutron scattering investigation of the crystal field excitations of NdCo<sub>5</sub>

F. de Almeida Passos <sup>1</sup>, G. J. Nilsen <sup>2,3</sup>, C. E. Patrick <sup>4</sup>, M. D. Le <sup>2</sup>, G. Balakrishnan <sup>5</sup>, Santosh Kumar <sup>5,6,\*</sup>,  
A. Thamizhavel <sup>6</sup>, D. R. Cornejo <sup>7</sup> and J. Larrea Jiménez <sup>1,†</sup>

<sup>1</sup>Laboratory for Quantum Matter under Extreme Conditions, Institute of Physics, University of São Paulo, São Paulo 05508-090, Brazil

<sup>2</sup>ISIS Pulsed Neutron and Muon Source, STFC Rutherford Appleton Laboratory, Didcot OX11 0QX, United Kingdom

<sup>3</sup>Department of Mathematics and Physics, University of Stavanger, 4036 Stavanger, Norway

<sup>4</sup>Department of Materials, University of Oxford, Oxford OX1 3PH, United Kingdom

<sup>5</sup>Department of Physics, University of Warwick, Coventry CV4 7AL, United Kingdom

<sup>6</sup>Department of Condensed Matter Physics and Materials Science, Tata Institute of Fundamental Research, Mumbai 400005, India

<sup>7</sup>Institute of Physics, University of São Paulo, São Paulo 05508-090, Brazil



(Received 1 June 2023; revised 27 September 2023; accepted 29 September 2023; published 7 November 2023)

We present an inelastic neutron scattering study of the crystal electric field (CEF) levels in the intermetallic ferrimagnets RECo<sub>5</sub> (RE = Nd and Y). In NdCo<sub>5</sub>, measurements at 5 K reveal two levels at approximately 28.9 and 52.9 meV. Crystal-field calculations including the exchange field  $B_{\text{exc}}$  from the Co sites account for both of these, as well as the spectrum at temperatures above the spin-reorientation transition at  $\sim 280$  K. In particular, it is found that both a large hexagonal crystal field parameter  $A_6^0(r^6)$  and  $B_{\text{exc}}$  are required to reproduce the data, with the latter having a much larger value than that deduced from previous computational and experimental studies. Our study sheds light on the delicate interplay of terms in the rare-earth Hamiltonian of RECo<sub>5</sub> systems, and is therefore expected to stimulate further experimental and computational work on the broader family of rare-earth permanent magnets.

DOI: [10.1103/PhysRevB.108.174409](https://doi.org/10.1103/PhysRevB.108.174409)

### I. INTRODUCTION

The rare-earth (RE) intermetallics RECo<sub>5</sub> have been extensively studied in the last three decades due to their attractive magnetic properties, which include high saturation magnetization and ordering temperature  $T_C$ , as well as strong magnetic anisotropy and large coercivity [1]. These can be understood as arising from the features of the rare-earth and transition-metal (TM) sublattices: the large saturation magnetization and high  $T_C$  are generated by the strongly interacting itinerant  $d$  electrons on the TM sublattice, while the localized RE  $f$  electrons, crystal electric field (CEF), and exchange field ( $B_{\text{exc}}$ ) from the TM site together produce the magnetic anisotropy [2].

Despite the fact that the CEF plays an important role in the mechanisms that underlie the magnetic properties of RECo<sub>5</sub> systems, the accurate determination of crystal field parameters (CFPs) in RECo<sub>5</sub> remains a challenge. Theoretical calculations based on *ab initio* methods have produced a wide range of CFPs and exchange fields [3,4], with a much narrower range of predicted physical properties, rendering comparisons with experiment ambiguous. Inelastic neutron scattering (INS) is one of the best tools to obtain both sets of parameters, but has only so far been applied to a few members of the RECo<sub>5</sub> family. This is at least in part because the exchange field  $B_{\text{exc}}$  both fully splits the RE ground-state

multiplet and mixes in higher multiplets, resulting in highly complex spectra. The availability of inelastic neutron scattering data is nevertheless expected to help to distinguish between theoretical parameter sets, and thus to identify the most promising theoretical tools to design the next generation of permanent magnets.

With this aim in mind, we here focus on the CEF in the NdCo<sub>5</sub> compound, which crystallizes in the hexagonal ( $P6/mmm$ ) space group symmetry with lattice parameters  $a = 5.0200(9)$  Å and  $c = 3.9664(4)$  Å, respectively [5]. Several studies using magnetization and neutron diffraction have already been performed on this compound: in particular, a spin-reorientation transition (SRT) between  $T_{SR1} = 240$  K and  $T_{SR2} = 280$  K [6] and a magnetic moment smaller than the expected saturation value have been observed [7]. Regarding the CEF, parameters from a range of theoretical calculations have been found to be broadly compatible with magnetization and other bulk data [3,4], with the best agreement at low temperature being obtained using dynamical mean field theory (DMFT) [3]. The latter work suggests that a strong hybridization between the Nd  $4f$  and Co  $3d$  orbitals generates a large 6th order CEF coefficient  $A_6^0(r^6)$ , which in turn increases the easy-plane anisotropy and reduces the low-temperature ordered moment on the Nd site.

Our study completes the picture of the CEF in NdCo<sub>5</sub> via inelastic neutron scattering experiments on both it and the isostructural compound YCo<sub>5</sub>, where the excitation spectrum is dominated by phonons. In NdCo<sub>5</sub>, two excitations at 28.9 meV and 52.9 meV are clearly observed at 5 K. Using previous calculations as a starting point, we fit the full inelastic neutron scattering spectrum to extract a set of CFPs

\*Present address: Department of Physics, Indian Institute of Technology Dharwad, Karnataka 580011, India.

†Corresponding author: [larrea@if.usp.br](mailto:larrea@if.usp.br)

and  $B_{\text{exc}}$  that explain the observed CEF excitations, including the spectrum above the spin-reorientation transition at 300 K. Remarkably, we find a much larger  $B_{\text{exc}}$  than previous *ab initio* calculations, as well as an  $A_6^6\langle r^6 \rangle$  coefficient in good agreement with the DMFT calculations discussed above.

## II. METHODS

### A. Experimental

Polycrystalline ingots of NdCo<sub>5</sub> and YCo<sub>5</sub> were synthesized by arc melting high purity Nd, Y, and Co elements in stoichiometric proportions on a water-cooled copper hearth in an argon atmosphere. The as-cast ingots were then ground to powder form for the neutron experiments. The phase purity of the powders was checked using powder x-ray diffraction, prior to the neutron measurements.

The inelastic neutron scattering measurements for both samples were performed on the MARI spectrometer at the ISIS Neutron and Muon Source, United Kingdom. Two sets of incident neutron energies were selected using a Fermi chopper and repetition rate multiplication:  $E_i = 180/30$  meV and  $E_i = 80/11$  meV. The corresponding resolutions at the elastic line were 7/0.7 meV and 3.8/0.3 meV, respectively. Data was collected at 5 K and 300 K in both configurations, and corrected for  $k_i/k_f$  to yield the dynamical structure factor  $S(|Q|, \Delta E = \hbar\omega)$ .

### B. Crystal Field Hamiltonian

The Hamiltonian used to fit the NdCo<sub>5</sub> spectra was

$$\mathcal{H} = \lambda \mathbf{L} \cdot \mathbf{S} + 2\mu_B \mathbf{B}_{\text{exc}} \cdot \mathbf{S} + \mathcal{H}_{\text{cf}}, \quad (1)$$

where the first term represents the spin-orbit coupling, the second the coupling between the exchange field and localized rare-earth spin moment, and the third the crystal field Hamiltonian. By choosing the quantization axis along the hexagonal  $c$  axis, the exchange field is taken to be parallel to the  $x$  axis (crystallographic  $a$  axis) below the spin-reorientation transition, and parallel to the  $z$  axis (crystallographic  $c$  axis) above it. For  $f$  electrons and the  $6/mmm$  site symmetry of the Nd atoms, four crystal field parameters are allowed: following the notation used in the RECo<sub>5</sub> literature, these are denoted  $A_2^0\langle r^2 \rangle$ ,  $A_4^0\langle r^4 \rangle$ ,  $A_6^0\langle r^6 \rangle$ , and  $A_6^6\langle r^6 \rangle$ . The Stevens and Wybourne conventions are related via  $A_k^q\langle r^k \rangle = \lambda_{kq} W_k^q$ , where  $\lambda_{kq}$  are multiplicative tabulated factors [8]. The crystal field Hamiltonian then reads

$$\mathcal{H}_{\text{cf}} = \Theta_2 A_2^0\langle r^2 \rangle \hat{O}_2^0 + \Theta_4 A_4^0\langle r^4 \rangle \hat{O}_4^0 + \Theta_6 [A_6^0\langle r^6 \rangle \hat{O}_6^0 + A_6^6\langle r^6 \rangle \hat{O}_6^6], \quad (2)$$

where  $\hat{O}_k^q$  are the Stevens operator equivalents. The dynamical structure factor  $S(|Q|, \Delta E)$  was evaluated using the standard expression for a powder in the dipole approximation

$$S(|Q|, \Delta E) = \frac{2}{3} \left( \frac{\gamma r_0}{2} \right)^2 g^2 f(|Q|)^2 \sum_{\nu} p_{\nu} \times \sum_{\nu'} \sum_{\alpha=\{x,y,z\}} |\langle \nu' | J_{\alpha} | \nu \rangle|^2 \delta(E_{\nu'} - E_{\nu} - \Delta E), \quad (3)$$

where  $p_{\nu}$  is the Boltzmann population factor for initial state  $|\nu\rangle$  in the  $|SLJm_J\rangle$  basis, and  $f(|Q|)^2$  is the Nd form factor. Given the large dimension of the parameter space, the least-squares fits were initialized using three literature parameter sets [3,4,9] (Table II) as well as the parameters obtained by performing a grid search in the lower dimensional space  $\{|B_{\text{exc}}|, A_2^0\langle r^2 \rangle, A_6^6\langle r^6 \rangle\}$  of the parameters that all previous calculations identify as most significant.

## III. RESULTS AND DISCUSSION

### A. Background subtraction

The dynamical structure factors  $S(|Q|, \Delta E)$  of NdCo<sub>5</sub> and YCo<sub>5</sub> at 5 K and  $E_i = 180$  and 80 meV are shown in Figs. 1(a)–1(d). At large wavevector transfers  $|Q|$ , the spectra of both materials are dominated by phonons, which appear in several strong bands between 15 and 60 meV. In the case of YCo<sub>5</sub>, no other features are observed in the  $(|Q|, \Delta E)$  range of our experiments; the magnons expected from the magnetic order are either too weak or too broad to observe. On the other hand, the  $E_i = 80$  meV and 180 meV spectra of NdCo<sub>5</sub> [Figs. 1(a) and 1(b)] reveal two features at  $\sim 50$  meV and  $\sim 30$  meV (see arrows), henceforth denoted as the high energy (HE) and low energy (LE) features. Both have  $|Q|$  dependences that are apparently consistent with magnetic excitations. Turning to the 300 K data [Figs. 1(e) and 1(f)],  $S(|Q|, \Delta E)$  for YCo<sub>5</sub> continues to be dominated by phonon scattering, while both of the lines observed for NdCo<sub>5</sub> at low temperature are absent from the spectrum. This drastic change will be shown to result from the spin-reorientation transition that switches the magnetization easy axis from the  $a$  axis to the  $c$  axis at  $T_{SR1}$  and  $T_{SR2}$ .

Before analyzing the spectra in detail, the CEF component of the scattering must first be isolated from the remainder. To achieve this, we compare two different approaches: subtracting either the YCo<sub>5</sub> data from the NdCo<sub>5</sub> data or using the scaled high- $|Q|$  phonon spectrum. Firstly, despite the difference in mass between Y and Nd, YCo<sub>5</sub> has a very similar phonon spectrum to NdCo<sub>5</sub> (see Fig. 1), with only a slight shift in phonon frequencies at low energies. The relative intensities are furthermore nearly identical across the whole energy range due to the scattering lengths of Y and Nd being very close in magnitude ( $b_Y = 7.75$  fm and  $b_{\text{Nd}} = 7.69$  fm). In addition, at sufficiently high  $|Q|$  the magnetic contribution should be negligible compared to the phonon scattering. Therefore, we also evaluate the phonon contribution to the NdCo<sub>5</sub> spectrum assuming that its low- $|Q|$  and high- $|Q|$  phonon scattering ratio scales in the same manner as in the isostructural compound YCo<sub>5</sub> [10], where the RE site is nonmagnetic. Figures 2(a) and 2(b) show excellent agreement between the NdCo<sub>5</sub> phonon background calculated using this scale function and the YCo<sub>5</sub> spectrum, making both suitable for removing the nonmagnetic contribution. The subtracted spectrum, shown along  $\Delta E$  in Fig. 2(c) and  $|Q|$  in Fig. 3 indicate that the phonon contribution is cleanly removed at energies above 20 meV.

In order to verify the magnetic origin of the observed features, we begin by analyzing the  $|Q|$  dependence of the two CEF excitations in NdCo<sub>5</sub>. Integrating the

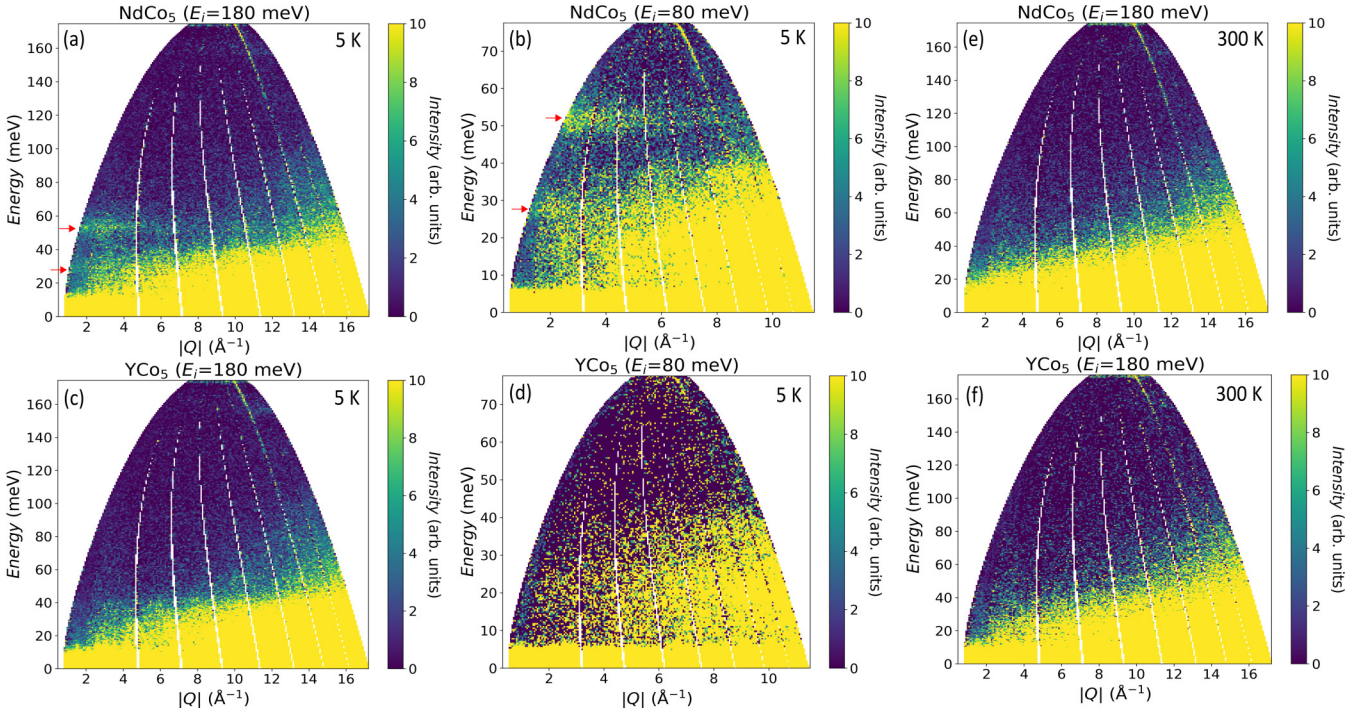


FIG. 1. Experimental inelastic neutron scattering intensity spectra of: (a) NdCo<sub>5</sub> at 5 K obtained using an incident neutron energy of  $E_i = 180$  meV; (b) NdCo<sub>5</sub> at 5 K obtained with  $E_i = 80$  meV; (c) YCo<sub>5</sub> at 5 K obtained with  $E_i = 180$  meV; (d) YCo<sub>5</sub> at 5 K obtained with  $E_i = 80$  meV; (e) NdCo<sub>5</sub> at 300 K obtained with  $E_i = 180$  meV, and (f) YCo<sub>5</sub> at 300 K obtained with  $E_i = 180$  meV. The red arrows in (a) and (b) indicate the two observed CEF excitations on the NdCo<sub>5</sub> spectra.

background-subtracted  $S(|Q|, \Delta E)$  over the energy transfer ranges of both, we obtain their  $|Q|$  dependence, as shown in Fig. 3. The red line in Fig. 3 is the squared magnetic form factor  $f(|Q|)^2$  for the Nd<sup>3+</sup> ion calculated in the dipole approximation  $f(|Q|) = \langle j_0 \rangle + c_2 \langle j_2 \rangle$  with  $c_2 = (2 - g_J)/g_J$  [11], where  $g_J$  is the Landé  $g$  factor. We can see that the intensities for both NdCo<sub>5</sub> CEF excitations decrease with  $|Q|$ , as expected for magnetic scattering, and that they also agree well with the Nd<sup>3+</sup> squared form factor, even at high  $|Q|$ , where the phonon intensity dominates. This provides additional reassurance that the background subtraction cleanly isolates the CEF magnetic scattering contribution, as well as showing that the strong  $f$ - $d$  hybridization suggested in Ref. [3] is nearly isotropic.

## B. Extracting CFPs

We now turn to cuts of  $S(|Q|, \Delta E)$  along  $\Delta E$  in the energy ranges  $20 < \Delta E < 40$  meV and  $40 < \Delta E < 70$  meV in Figs. 2(a) and 2(b). These were obtained by integrating the  $E_i = 180$  meV data at 5 K over the  $|Q|$  ranges  $1.0 < Q < 4.5$  Å<sup>-1</sup>,  $1.6 < Q < 5.0$  Å<sup>-1</sup>, respectively. Since the cuts run over different  $|Q|$  ranges, the intensity was corrected by dividing it by the ratio of  $f(|Q|)^2$  integrated over the  $|Q|$  ranges above and  $\int_0^\infty f(|Q|)^2 dQ$ . This is justified by the fact that the  $|Q|$  dependences in Figs. 3(a) and 3(b) are in good agreement with  $f(|Q|)^2$  for Nd<sup>3+</sup>. Firstly, it is evident that both the LE and HE features have a roughly Lorentzian profile and are considerably broader than the (Gaussian) instrumental resolution,

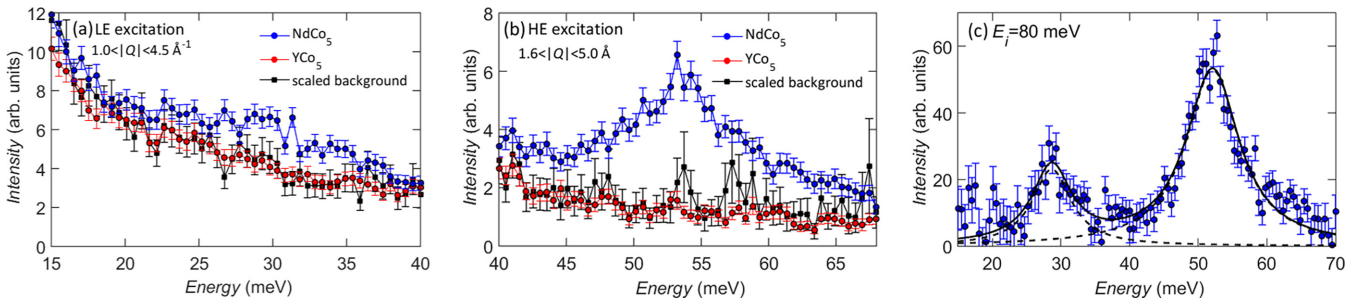


FIG. 2. (a) Dynamical structure factor  $S(|Q|, \Delta E)$  of NdCo<sub>5</sub> and YCo<sub>5</sub> at 5 K obtained by integrating the  $E_i = 180$  meV data over a  $Q$  range of  $1.0 < Q < 4.5$  Å<sup>-1</sup> showing the peak in the NdCo<sub>5</sub> spectrum corresponding to the LE CEF excitation. (b) Energy spectra of NdCo<sub>5</sub> and YCo<sub>5</sub> at 5 K obtained integrating the  $E_i = 180$  meV data over a  $Q$  range of  $1.6 < Q < 5.0$  Å<sup>-1</sup> showing the peak in the NdCo<sub>5</sub> spectrum corresponding to the HE CEF excitation. (c) NdCo<sub>5</sub> background-subtracted spectrum using  $E_i = 80$ , and after intensity correction to account for the different  $|Q|$  integration ranges (filled circles) fitted by a Lorentzian function (solid line).

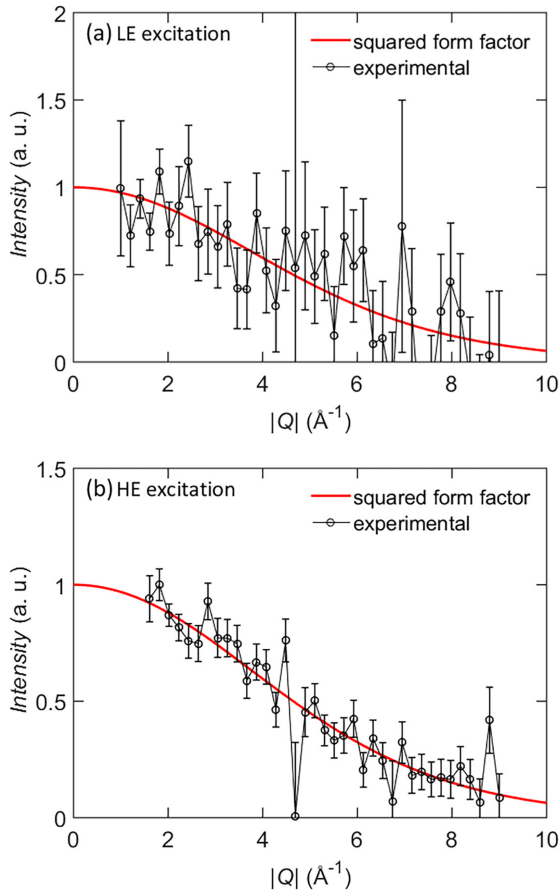


FIG. 3. Normalized scattered intensities as a function of  $|Q|$  of  $\text{NdCo}_5$  spectrum measured with  $E_i = 180$  meV at 5 K obtained integrating over the (a) LE peak range (20 to 40 meV) and (b) HE peak range (40 to 70 meV). The solid red line shows the calculated squared form factor for the  $\text{Nd}^{3+}$  ion using the analytical approximation [11].

which is estimated to be 5.8 meV for the LE peak and 5.2 meV for the high-energy HE peak for the  $E_i = 180$  meV data, and 2.5 and 1.7 meV for the LE and HE peaks, respectively, for the  $E_i = 80$  meV data. They are also broad compared to the CEF excitations in  $\text{SmCo}_5$  [12]. This justifies the choice of a model containing two Lorentzians to fit the experimental data.

This broadening of the CEF excitations has several possible origins: (i) dispersion due to long-range interactions between the localized  $\text{Nd}^{3+}$   $f$  electrons mediated by the conduction electrons [13]; (ii) magnetoelastic coupling between the CEF excitations and the phonons [14]; and (iii)  $f$ - $d$  exchange between the localized  $f$  electrons and the itinerant  $d$  electrons (Landau damping), in a manner analogous to the  $f$ - $s$  broadening mechanism proposed in [15]. Since the current experiments were performed on polycrystalline samples, we were unable to resolve the dispersion of the CEF excitations, although powder averaging would be unlikely to produce the Lorentzian lineshape observed experimentally. This means that (i) is almost certainly not the dominant source of broadening. For (ii), the similarity of the phonon spectra of  $\text{YCo}_5$ , where no magnetoelastic coupling is expected, and  $\text{NdCo}_5$  at all  $|Q|$  suggests that any magnetoelastic effects present should be too small to explain the large broadening of both the LE and

TABLE I. Fitted Lorentzian function parameters for each peak in  $\text{NdCo}_5$  spectrum at 5 K and  $E_i = 80$  meV.

	Center (meV)	Intensity	FWHM (meV)
Low-energy peak	28.6(4)	249(28)	7(1)
High-energy peak	52.1(2)	785(26)	9.4(4)

HE features.<sup>1</sup> Finally, regarding (iii), significant broadening effects have been observed in several other itinerant rare-earth systems, where they were ascribed to coupling between the localized  $4f$  moments and electron-hole excitations in the valence  $5s$  band [15]. If a similar mechanism couples the Nd moments to the Co  $3d$  band in  $\text{NdCo}_5$ , we expect that only the temperature-independent term  $\propto K_{ex}\mathcal{N}(0)$  is active, as the Kramers degeneracy is broken by the exchange field.

The  $\text{NdCo}_5$  background-subtracted spectra for both the  $E_i = 80$  and 180 meV data were thus fitted with two Lorentzian functions to extract the transition energies and intensities. The Lorentzian intensities, widths, and positions were allowed to vary freely during this fitting. Attempts to fit three Lorentzian were unstable. Table I shows the peak parameters for the  $E_i = 80$  meV data.

Thereafter, the fits of the model parameters from the Hamiltonian given in Sec. II B were carried out using a custom Python code, as well as SPECTRE and PyCrystalField software packages [8,16]. In the first case, the basis was truncated to the three lowest  $J$  multiplets of the  $^4I$  term ( $J = 9/2, 11/2, 13/2$ ), giving 36 basis states. For the SPECTRE fits, both the ground state  $^4I$  and excited  $^4F$  terms were considered. Since SPECTRE uses the Wybourne operator equivalents  $\hat{C}_q^k$  and coefficients  $W_k^q$ , the latter were converted to  $A_k^q\langle r^k \rangle$  using tabulated factors (see Appendix A 1). In both cases, the peak positions and integrated intensities of the LE and HE features at 5 K were used to fit the CEF Hamiltonian parameters. Both fittings showed that the LE feature should consist of two unresolved transitions. Therefore, we also performed the fittings with PyCrystalField, which has the advantage of fitting the whole neutron spectrum without having to assume unresolved transitions. For the PyCrystalField fitting, we used a Lorentzian peak profile and the widths of the peaks were constrained to the FWHM values obtained by the Lorentzian fitting of the spectrum (Table I). In all cases, the fittings were performed using the intermediate coupling scheme with a spin-orbit constant  $\lambda$  of 540 K [4]. During the fitting procedure, the neutron spectrum was found to be strongly sensitive to just three parameters: the  $A_2^0\langle r^2 \rangle$  and  $A_6^6\langle r^6 \rangle$  CFPs, and the exchange field  $B_{exc}$ . Due to the large width of the peaks—which renders reliable extraction of intensities challenging—and the small number of measured levels, the remaining discussion will center around the parameters extracted from PyCrystalField.

Table II shows the values obtained for the CFPs as well as the magnitude of the exchange field  $B_{exc}$ , whose direction is along the  $a$  axis below the lower spin-reorientation transition

<sup>1</sup>However, magneto-elastic coupling cannot be conclusively excluded without determining the phonon dispersion.

TABLE II. NdCo<sub>5</sub> crystal-field parameters, and magnitude of the exchange field ( $B_{\text{exc}}$ ), whose direction is along the  $a$  axis below the SRT, obtained by fitting to the CEF transitions observed experimentally at 5 K. The CFPs are in the Stevens notation. We compare the experimental values obtained here with some previous theoretical works, and the parameters obtained by Zhao *et al.* [9] which were obtained by fitting magnetization curves.

	$A_2^0\langle r^2 \rangle$ (K)	$A_4^0\langle r^4 \rangle$ (K)	$A_6^0\langle r^6 \rangle$ (K)	$A_6^6\langle r^6 \rangle$ (K)	$B_{\text{exc}}$ (T)
custom Python code	-300	0	10	900	535
SPECTRE	$-460 \pm 170$	0	0	$1026 \pm 60$	$506 \pm 5$
PyCrystalField	$-240 \pm 100$	0	0	$1150 \pm 60$	$470 \pm 30$
Patrick and Staunton [4]	-415	-26	5	146	252
Pourovskii <i>et al.</i> [3]	-285	-33	36	1134	292
Zhao <i>et al.</i> [9]	-510	0	7	143	558

temperature  $T_{\text{SRT}}$ . Although there are some differences mainly in the  $A_2^0\langle r^2 \rangle$  among the fitted parameters, all three approaches suggest a large  $A_6^6\langle r^6 \rangle$  and  $B_{\text{exc}}$ . Choosing the quantization axis along the crystallographic  $a$  axis for better comparison with previous references, we obtain the following ground state of the Nd<sup>3+</sup> in NdCo<sub>5</sub> for the PyCrystalField parameter set in  $|J, m_J\rangle$  basis:

$$\Psi_{\text{GS}}^{\text{Nd}} = -0.92|9/2, -9/2\rangle - 0.36|9/2, -5/2\rangle + 0.13|11/2, -9/2\rangle + 0.09|11/2, -5/2\rangle. \quad (4)$$

We can notice from the ground-state function a significant contribution from the higher multiplet  $J = 11/2$ , which corroborates the importance of including  $J$  mixing to describe this system. Table V in the Appendix A 2 shows the obtained eigenvalues and respective eigenstates. This  $J$  mixing is a consequence mainly from the large  $A_6^6\langle r^6 \rangle$  CFP obtained [3].

Figure 4 depicts the comparison between intensities using CFPs obtained from previous works [3,4,9] and from our fitting using PyCrystalField. Of the spectra calculated using the CFPs derived from first principles, the DMFT results of Ref. [3] provide the closest fit at 5 K, which can be attributed to the large  $A_6^6\langle r^6 \rangle$  parameter obtained in that work. However, the exchange field derived in Ref. [3] is not sufficiently large to reproduce the positions of the peaks in the spectrum, even though it was shown to produce magnetization properties consistent with experiment.

Having obtained a set of parameters that reproduces the experimentally observed CEF excitations at 5 K, we now check the agreement of these parameters with our results at high temperature. At 300 K, above the SRT, the NdCo<sub>5</sub> magnetization easy axis is parallel to the crystallographic  $c$  axis. Rotating the exchange-field direction to the  $c$  axis at 300 K, and assuming that the CFPs and  $|B_{\text{exc}}|$  do not change significantly with temperature, we obtain the spectrum shown in Fig. 4(b) considering a FWHM of 10 meV for the peaks at this temperature. We can see that the parameter set obtained by fitting the 5 K data also agrees well with the experimental spectrum at 300 K, showing no peaks above 25 meV. However, due to thermal broadening of the peaks and the experimental resolution close to the elastic line, it was not possible to experimentally resolve the peaks below 25 meV.

### C. Comparison of CFPs

All previous studies agree that the  $A_2^0\langle r^2 \rangle$  is negative, which drives the basal-plane anisotropy. The  $A_2^0\langle r^2 \rangle$  value ob-

tained by SPECTRE is somewhat larger in magnitude than the values calculated from first principles in Refs. [3,4] but consistent with the larger value obtained in Ref. [9] based on the fitting of magnetization data. We further find that both  $A_4^0\langle r^4 \rangle$  and  $A_6^0\langle r^6 \rangle$  do not significantly affect the excitation spectrum, so they cannot be strongly constrained by our measurements. The  $A_6^0\langle r^6 \rangle$  in the custom Python code was introduced to

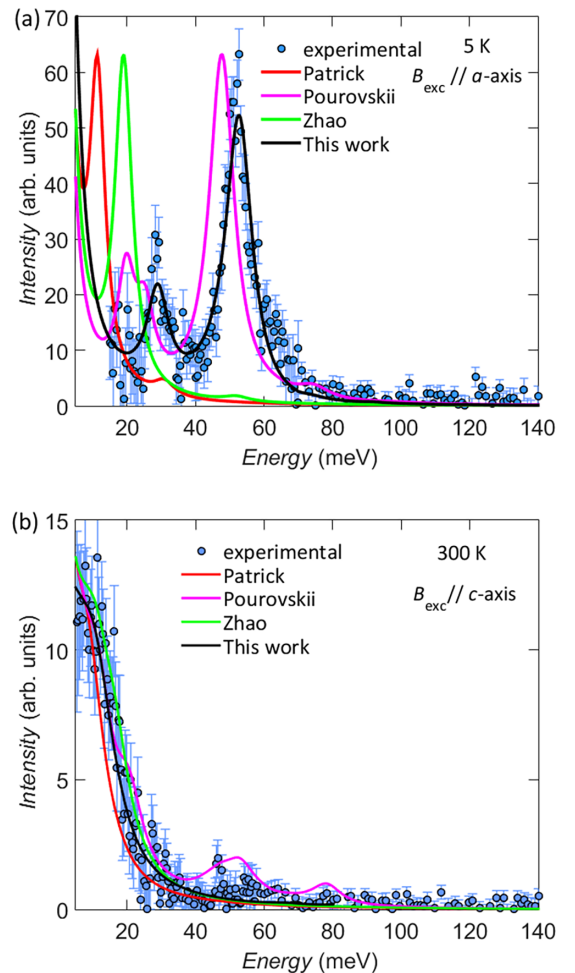


FIG. 4. Fitting to the experimental spectrum using PyCrystalField and calculated neutron spectra using different parameter sets from previous references [3,4,9] compared with the experimental data at (a) 5 K and (b) 300 K, both measured with a neutron incident energy of 80 meV.

improve the agreement with the magnetization data (see Appendix A 3). However, the spectrum is sensitive to both  $A_6^0\langle r^6 \rangle$  and  $B_{\text{exc}}$ , leading to the best fit values of 1150 K and 470 T, respectively. Pourousskii *et al.* [3] found a similarly large value of  $A_6^0\langle r^6 \rangle$  using their DMFT framework, and argued that this term also accounts for the nonsaturated Nd moments at zero temperature [7]. In fact, from the PyCrystalField parameter set, we obtain a value of  $2.90 \mu_B$  for the Nd ground state magnetic moment, which is significantly lower than the  ${}^4I_{9/2}$  saturated moment and in good agreement with the experimental value of  $2.82 \mu_B$  from Ref. [7]. Relatively large values of  $l = 6$  coefficients are also found necessary to explain, e.g., the spin reorientation in  $\text{Nd}_2\text{Fe}_{14}\text{B}$  [17]. Calculations which do not explicitly include hybridization of the  $4f$  electrons with their environment (such as the yttrium-analogue model of Ref. [4]) do not produce these large higher-order CFPs. The analysis of our inelastic neutron spectra thus corroborates the idea that a standard assumption of crystal field theory—that the strongly localized  $f$  electrons do not themselves affect the crystal field—does not hold in  $\text{NdCo}_5$ .

We finally note that the  $B_{\text{exc}}$  extracted from the fit is considerably larger than the estimations from Refs. [3,4]. This, together with the large  $A_2^0\langle r^2 \rangle$  is expected to cause an overestimation of the SRT temperatures  $T_{SR1}$  and  $T_{SR2}$  compared to both calculations of the SRT using previous parameter sets and experiments. The former, however, do not consider a range of possible additional terms in the Hamiltonian, including exchange anisotropy and the anisotropy on the Co sites [18]. Some of these terms can compensate the influence of  $B_{\text{exc}}$  and  $A_2^0\langle r^2 \rangle$  and restore the predicted  $T_{SR1}$  and  $T_{SR2}$  to the experimentally observed temperatures.

#### IV. CONCLUSION

We have performed inelastic neutron scattering to investigate the crystal electric field (CEF) levels in the intermetallic ferrimagnets  $\text{RECo}_5$  ( $\text{RE} = \text{Nd}$  and  $\text{Y}$ ). The large  $A_6^0\langle r^6 \rangle$  extracted from our experimental data as well as the large linewidths of the inelastic peaks highlight the importance of the interaction between the localized  $f$  electrons and itinerant  $d$  electrons for both the CEF and magnetic anisotropic interactions. The former is in good agreement with previous calculations [3], although the exchange field is considerably higher than previously reported values. In light of the ongoing discussion around the magnetism of other technologically relevant rare-earth intermetallics, including the  $\text{Nd}_2\text{Fe}_{14}\text{B}$  family [19,20], we are hopeful that our approach to fitting full inelastic neutron CEF spectra can help to shed further light on the interplay of interactions that generate their interesting magnetic properties.

TABLE III.  $\text{NdCo}_5$  crystal-field parameters in the Stevens convention and magnitude of the exchange field obtained by fitting the experimental spectrum at 5 K using PyCrystalField in the intermediate-coupling scheme.

$B_2^0$ (meV)	$B_6^0$ (meV)	$B_{\text{exc}}$ (T)
0.08458726	-0.00112046	470

TABLE IV.  $\text{NdCo}_5$  crystal-field parameters in the Wybourne convention and magnitude of the exchange field obtained by fitting the experimental spectrum at 5 K using SPECTRE software in the intermediate-coupling scheme.

$W_2^0$ (meV)	$W_6^0$ (meV)	$B_{\text{exc}}$ (meV)
-93	83	31

#### ACKNOWLEDGMENTS

The authors acknowledge A. Scheie for helping with the implementation of the exchange-field interaction in PyCrystalField. F.A.P., G.J.N., and J.L.J. acknowledge Grants No. 2019/24711-0, No. 2019/24797-1, and No. 2018/08845-3, São Paulo Research Foundation (FAPESP). J.L.J. acknowledges Centro Nacional de Desenvolvimento Científico e Tecnológico (CNPq) Grant No. 31005/2021-6. This study was financed in part by the Coordenação de Aperfeiçoamento de Pessoal de Nível Superior - Brasil (CAPES) - Finance code 001. The work at the university of Warwick was supported

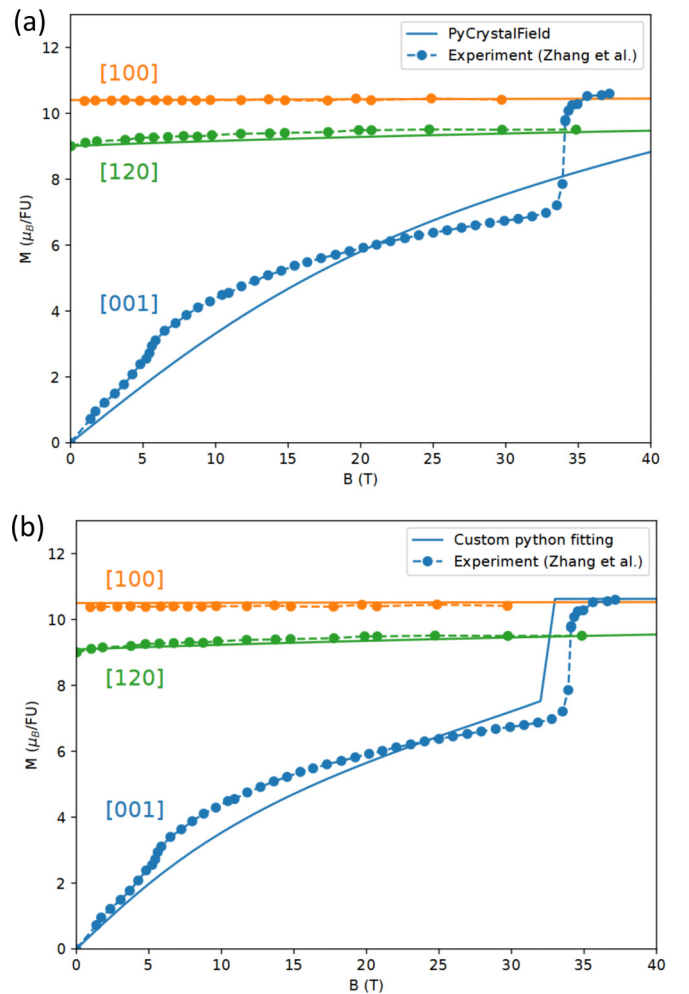


FIG. 5. Magnetization curves calculated using either the PyCrystalField or custom Python code parameters, compared to experimental measurements for a  $\text{NdCo}_5$  single crystal reported by Zhang *et al.* [24] at 4.2 K.

TABLE V. Eigenvalues and eigenstates in the  $J$  basis for the `PyCrystalField` parameters set in Table II obtained at 5 K. Note that here the quantization axis was chosen along the  $a$  axis, as adopted in other references. To obtain these eigenvectors, we rotated the CFPs in Table II from  $z||c$  to  $z||a$  using the rotation matrices in Ref. [22] and therefore the exchange field was also rotated to the  $z$  axis to continue parallel to the crystallographic  $a$ -axis.

Eigenvalues (meV)	Eigenstates $ J, m_J\rangle$
0.00	$-0.92 9/2, -9/2\rangle - 0.36 9/2, -5/2\rangle + 0.13 11/2, -9/2\rangle + 0.09 11/2, -5/2\rangle$
28.33	$0.88 9/2, -5/2\rangle - 0.36 9/2, -9/2\rangle - 0.26 9/2, -1/2\rangle - 0.12 11/2, -5/2\rangle$
29.25	$0.71 9/2, -3/2\rangle - 0.69 9/2, -7/2\rangle - 0.16 11/2, -3/2\rangle - 0.05 9/2, 5/2\rangle$
52.48	$0.72 9/2, -7/2\rangle + 0.67 9/2, -3/2\rangle - 0.14 11/2, -3/2\rangle + 0.07 9/2, 1/2\rangle$
74.12	$-0.89 9/2, -1/2\rangle - 0.28 9/2, 3/2\rangle - 0.26 9/2, -5/2\rangle + 0.19 11/2, -1/2\rangle$
91.80	$0.89 9/2, 1/2\rangle - 0.42 9/2, 5/2\rangle - 0.13 11/2, 1/2\rangle - 0.07 9/2, -3/2\rangle$
92.69	$-0.91 9/2, 3/2\rangle + 0.30 9/2, -1/2\rangle + 0.26 9/2, 7/2\rangle + 0.11 11/2, 3/2\rangle$
99.27	$-0.88 9/2, 5/2\rangle - 0.41 9/2, 1/2\rangle + 0.18 11/2, 5/2\rangle - 0.11 9/2, 9/2\rangle$
134.04	$0.93 9/2, 7/2\rangle + 0.27 9/2, 3/2\rangle - 0.25 11/2, 7/2\rangle - 0.06 11/2, 3/2\rangle$
140.58	$-0.99 9/2, 9/2\rangle + 0.10 11/2, 9/2\rangle - 0.09 11/2, 5/2\rangle + 0.07 9/2, 1/2\rangle$

through Grants No. EP/M02941/1 and No. EP/T005963/1 from Engineering and Physical Sciences Research Council (EPSRC), United Kingdom.

## APPENDIX

### 1. CFPs notation

The CFPs in Table II are in the Stevens notation as originally derived by Stevens [21]. Although `PyCrystalField` also uses the Stevens convention, it defines the CFPs as  $B_k^q = A_k^q \langle r^k \rangle \Theta_k$ , where  $\Theta_k$  are the Stevens factors [21]. On the other hand, SPECTRE uses the CFPs  $W_k^q = A_k^q \langle r^k \rangle / \lambda_{kq}$  in the Wybourne notation, where  $\lambda_{kq}$  are tabulated factors [8]. Tables III and IV show the CFPs as obtained by `PyCrystalField` and SPECTRE, respectively, prior to performing any conversion.

### 2. Eigenvalues and Eigenstates

Table V show the eigenvalues with respective eigenvectors (up to the fourth largest term) in the  $|SLJm_J\rangle$  basis obtained for the `PyCrystalField` parameters set with the quantization axis along the  $a$  axis for better comparison with previous references [3,7]. The eigenvectors were obtained by converting the

eigenvectors from `PyCrystalField`, which were in the LS basis, to the  $J$  basis using the Clebsch-Gordan coefficients.

### 3. Magnetization curves

Figure 5 shows the comparison between the experimental and the calculated magnetization curves for the different directions of applied fields, as indicated, using both `PyCrystalField` and custom Python code parameter sets. The experimental measurements on single crystals at 4.2 K were taken from Ref. [23]. Importantly, although the CEF excitation spectrum is rather insensitive to  $A_6^0 \langle r^6 \rangle$ , the parameter does play an important role in determining whether or not the magnetization undergoes a sudden jump at approximately 35 T when the field is applied in the [001] direction. If this parameter is zero, as with the `PyCrystalField` parameters, the magnetization instead rotates continuously and slowly towards the  $c$  axis, with no jump observed.

The magnetization curves were calculated following the approach demonstrated, e.g., in Ref. [9]. For the parameter values of  $K_{1, TM}$  and  $M_{Co}$ , we used the same values as in Ref. [3]: a calculated value of  $7.5 \mu_B/FU$  for  $M_{Co}$  and a value of  $3.88 \text{ meV}/FU$  ( $45 \text{ K}/FU$ ) for  $K_{1, TM}$ , as measured experimentally at 4.2 K for  $YCo_5$  [25].

- 
- [1] K. Strnat, *IEEE Trans. Magn.* **6**, 182 (1970).  
[2] M. Richter, *J. Phys. D* **31**, 1017 (1998).  
[3] L. V. Pourovskii, J. Boust, R. Ballou, G. G. Eslava, and D. Givord, *Phys. Rev. B* **101**, 214433 (2020).  
[4] C. E. Patrick and J. B. Staunton, *Phys. Rev. Mater.* **3**, 101401(R) (2019).  
[5] K. Wang, M. Zhang, J. Liu, H. Luo, and J. Sun, *J. Appl. Phys.* **125**, 243901 (2019).  
[6] H. Klein, A. Menth, and R. Perkins, *Physica B+C* **80**, 153 (1975).  
[7] J. Alameda, D. Givord, R. Lemaire, Q. Lu, S. Palmer, and F. Tasset, *Le J. Phys. Colloques* **43**, C7-133 (1982).  
[8] A. T. Boothroyd, SPECTRE - a program for calculating spectroscopic properties of rare earth ions in crystals (1990-2014).  
[9] Z. Tie-song, J. Han-min, G. Guang-hua, H. Xiu-feng, and C. Hong, *Phys. Rev. B* **43**, 8593 (1991).  
[10] A. P. Murani, *Phys. Rev. B* **50**, 9882 (1994).  
[11] A. Freeman and J. Desclaux, *J. Magn. Magn. Mater.* **12**, 11 (1979).  
[12] P. Tils, M. Loewenhaupt, K. Buschow, and R. Eccleston, *J. Alloys Compd.* **289**, 28 (1999).  
[13] K. W. Becker, P. Fulde, and J. Keller, *Zeitschrift Phys. B Condens. Matter* **28**, 9 (1977).  
[14] P. Fulde and M. Loewenhaupt, *Adv. Phys.* **34**, 589 (1985).  
[15] K. W. Becker, P. Fulde, and J. Keller, *J. Phys. D* **28**, 9 (1977).  
[16] A. Scheie, *J. Appl. Crystallogr.* **54**, 356 (2021).  
[17] J. F. Herbst, *Rev. Mod. Phys.* **63**, 819 (1991).

- [18] J.-X. Zhu, M. Janoschek, R. Rosenberg, F. Ronning, J. D. Thompson, M. A. Torrez, E. D. Bauer, and C. D. Batista, *Phys. Rev. X* **4**, 021027 (2014).
- [19] J. Bouaziz, C. E. Patrick, and J. B. Staunton, *Phys. Rev. B* **107**, L020401 (2023).
- [20] J. Boust, A. Aubert, B. Fayyazi, K. P. Skokov, Y. Skourski, O. Gutfleisch, and L. V. Pourovskii, *Phys. Rev. Mater.* **6**, 084410 (2022).
- [21] K. W. H. Stevens, *Proc. Phys. Soc. A* **65**, 209 (1952).
- [22] C. Rudowicz, *J. Phys. C* **18**, 1415 (1985).
- [23] F. Zhang, D. Gignoux, D. Schmitt, J. Franse, and F. Kayzel, *J. Magn. Magn. Mater.* **136**, 245 (1994).
- [24] R. Zhang, B. Singh, C. Lane, J. Kidd, Y. Zhang, B. Barbiellini, R. S. Markiewicz, A. Bansil, and J. Sun, *Phys. Rev. B* **105**, 195134 (2022).
- [25] J. Alameda, D. Givord, R. Lemaire, and Q. Lu, *J. Appl. Phys.* **52**, 2079 (1981).